

# Quantum Magnetic Skyrmion Operator

Andreas Haller,<sup>1</sup> Sebastián A. Díaz,<sup>2</sup> Wolfgang Belzig,<sup>2</sup> and Thomas L. Schmidt<sup>1</sup>

<sup>1</sup>*Department of Physics and Materials Science, University of Luxembourg, 1511 Luxembourg, Luxembourg*

<sup>2</sup>*Department of Physics, University of Konstanz, 78457 Konstanz, Germany*

(Dated: March 18, 2024)

We propose a variational wave function to represent quantum skyrmions as bosonic operators. The operator faithfully reproduces two fundamental features of quantum skyrmions: their classical magnetic order and a “quantum cloud” of local spin-flip excitations. Using exact numerical simulations of the ground states of a 2D chiral magnetic model, we find two regions in the single-skyrmion state diagram distinguished by their leading quantum corrections. We use matrix product state simulations of the adiabatic braiding of two skyrmions to verify that the operator representation of skyrmions is valid at large inter-skyrmion distances. Our work demonstrates that skyrmions can be approximately coarse-grained and represented by bosonic quasiparticles, which paves the way toward a field theory of many-skyrmion quantum phases which, unlike other approaches, incorporates the microscopic quantum fluctuations of individual skyrmions.

*Introduction.*— Magnetic skyrmions are topologically nontrivial spin configurations which often arise in non-centrosymmetric magnetic materials [1–4] and have mostly admitted a description in terms of classical magnetic moments [5]. However, by now several materials have been found where the sizes of individual skyrmions can be on the order of the spacing of the underlying atomic lattice [6, 7]. This makes it necessary to explore their properties based on the underlying quantum mechanical models. Quantum fluctuations, superposition states, and entanglement become unavoidable and fascinating features of quantum magnetic skyrmions that still remain largely unexplored despite their relevance for the emerging proposals of skyrmion-based quantum technologies. Such applications include proposals on the potential use of skyrmions as qubits in frustrated magnets [8, 9] and as mobile impurities to implement topological quantum computing in magnet-superconductor heterostructures [10, 11]. The fundamental quantum features of magnetic skyrmions eventually render a classical description unsuitable, hence calling for a new and inherently quantum mechanical theoretical framework.

Quantum magnetic skyrmions emerge, for instance, as the many-body ground state of ferromagnetic spin-1/2 Heisenberg models with either Dzyaloshinskii-Moriya interactions or frustration due to antiferromagnetic next-nearest neighbor couplings. Since an exact numerical diagonalization of such spin Hamiltonians becomes prohibitive for a large number of lattice sites, the theoretical description of quantum magnetic skyrmions has relied mainly on alternative approaches. Near the classical limit, collective coordinates together with path integral techniques have been employed to model quantum skyrmion nucleation [12, 13] and quantum skyrmion dynamics [14, 15]. These approaches, unfortunately, are inadequate to model systems of interest for quantum technologies: quantum skyrmions in large numbers and in the deep quantum regime. In the deep quantum regime, quantitative predictions for few-skyrmion systems can be made based on exact diagonalization [16–20], neural network states [21, 22], dynamical mean-field simu-

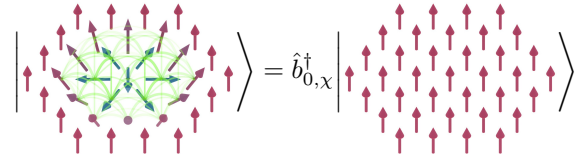


FIG. 1. Creation of a quantum magnetic skyrmion. The quantum magnetic skyrmion operator  $\hat{b}_{0,x}^\dagger$  acts on the field-polarized vacuum state to create a quantum magnetic skyrmion. By construction, the operator captures the fundamental features: classical magnetic order (arrows) and quantum fluctuations visualized by pairwise spin entanglement (green lines).

lations [23], and density matrix renormalization group simulations [24].

In this work, we develop a theoretical framework that makes it possible to describe this regime. It is based on the construction of creation and annihilation operators of quantum skyrmions and thus treats magnetic skyrmions as quantum quasiparticles. This compact and elegant theoretical framework captures the quantum skyrmion’s defining features: a classical magnetic order with quantum fluctuations. Constructing this operator allows us to clarify the role played by quantum fluctuations and to determine the range of validity of the semiclassical approximation. The quantum magnetic skyrmion operator is a natural and computationally efficient starting point to model skyrmion-skyrmion interactions and quantum many-body skyrmion phenomena.

*Quantum Skyrmion Operator.*— The proposed construction of the quantum skyrmion operator relies on the assumption that a magnetic quantum skyrmion has a typical magnetic order in the local spin expectation values. This includes cases where the norm of the vector of spin expectation values is not quantized to the quantum spin  $s$ , and we seek to faithfully capture the quantum fluctuations around the magnetic order. In the following, we focus on the special case of  $s = 1/2$ , but our construction admits a natural extension to any spin  $s$ .

We start by defining a product of local spin rotations

$$\hat{R}_{\bar{0}}(\boldsymbol{\theta}, \boldsymbol{\phi}) = \prod_{j \neq 0} e^{-i\phi_j \hat{S}_{j,z}} e^{-i\theta_j \hat{S}_{j,y}}, \quad (1)$$

where the subscript  $\bar{0}$  indicates that the site  $j = 0$  is excluded from the operator product. For suitably chosen angles  $\phi_j$  and  $\theta_j$ , we may write a classical magnetic skyrmion, which is represented by a product state in real space, in the form

$$|\Psi_c(\boldsymbol{\theta}, \boldsymbol{\phi})\rangle = \hat{R}_{\bar{0}}(\boldsymbol{\theta}, \boldsymbol{\phi}) \hat{S}_0^- |0\rangle \quad (2)$$

where the fully spin-polarized state  $|0\rangle = \otimes |\uparrow\rangle_i$  acts as the vacuum state and the spin at site  $j = 0$  is flipped with respect to the polarized environment. We can therefore interpret  $\hat{b}_{0,0}^\dagger = \hat{R}_{\bar{0}} \hat{S}_0^-$  as a creation operator for the classical skyrmion  $|\Psi_c\rangle$  from the vacuum  $|0\rangle$ .

Since  $[\hat{R}_{\bar{0}}, \hat{S}_0^-] = 0$ , the local commutation relations of  $\hat{b}_{0,0}^\dagger$  are given by  $\{\hat{b}_{0,0}, \hat{b}_{0,0}^\dagger\} = 1$  and  $[\hat{b}_{0,0}, \hat{b}_{0,0}^\dagger] = 2\hat{S}_{0,z}$ . We can analogously define creation operators for all sites of the lattice by  $\hat{b}_{i,0}^\dagger = \hat{R}_{\bar{i}} \hat{S}_i^-$  by shifting all operators from site 0 to site  $i$ . Clearly, the commutator of  $\hat{b}_{i,0}$  and  $\hat{b}_{j,0}^\dagger$  (or  $\hat{b}_{j,0}$ ) vanishes if sites  $i$  and  $j$  are distant enough such that the local rotations  $\phi_j, \theta_j$  contributing to  $\hat{R}_{\bar{i}}$  and  $\hat{R}_{\bar{j}}$  act on disjoint sets of sites.

To incorporate quantum fluctuations around the classical order, we define the following quantum skyrmion creation operator,

$$\hat{b}_{i,\chi}^\dagger = \frac{\hat{R}_{\bar{i}}}{\sqrt{\sum_{k=0}^{\chi} |w_k|^2}} \sum_{k=0}^{\chi} w_k \left( \prod_j (\hat{S}_j^-)^{n_{k,j}} \right), \quad (3)$$

which is the central object of this paper. The complex scalar weights  $\{w_0, \dots, w_\chi\}$  are sorted by descending absolute value,  $|w_i| \geq |w_{i+1}|$ ,  $\mathbf{n}_k \in \{0, 1\}^{\otimes N}$  is a vector representing the number of ladder operators in the product of spin flips, and  $\chi$  is a so far arbitrary integer which is bounded by the dimension of the Hilbert space. Equation (3) is motivated by the observation that magnetically ordered quantum skyrmion ground states centered at position  $i$  are in general surrounded by a ‘‘cloud’’ of spin flip fluctuations [21, 22, 24]. For semiclassical skyrmion profiles one has  $\mathbf{n}_0$  with  $n_{0,i} = 1$  and  $n_{0,j \neq i} = 0$  associated with the leading contribution  $|w_0| > |w_{k \neq 0}|$  from the classical order. The precise form of other occupation vectors  $\mathbf{n}_{k \neq 0}$ , corresponding to the ‘‘quantum cloud’’, remain undetermined and are model-dependent. It is straightforward to recognize that the local commutation relation of quantum skyrmion operators is approximately given by

$$[\hat{b}_{i,\chi}, \hat{b}_{i,\chi}^\dagger] \approx \frac{|w_0|^2}{\sum_k |w_k|^2} 2\hat{S}_{i,z}, \quad \{\hat{b}_{i,\chi}, \hat{b}_{i,\chi}^\dagger\} \approx \frac{|w_0|^2}{\sum_k |w_k|^2}, \quad (4)$$

together with

$$[\hat{b}_{i,\chi}, \hat{b}_{j,\chi}^\dagger] = 0 \text{ for } |\mathbf{R}_j - \mathbf{R}_i| > r_c \quad (5)$$

in which  $r_c$  denotes the radius of the skyrmion profile. In total, one can therefore interpret the quantum skyrmion operator as a bosonic entity, but with a constraint on the local Hilbert space dictated by Eq. (4). Using matrix product state simulations, it is possible to extract the phase after an adiabatic exchange of a system containing two quantum skyrmions, and we find that the exchange phase is compatible with Eq. (5) (see Supplemental Material [25]). Moreover, the local ‘‘hard-core’’ constraint of Eq. (4) agrees with the numerical observation that many-skyrmion ground states are composed of skyrmion crystals and liquids [24]. In principle, an operator of the form Eq. (3) can be used to construct a complete basis of the Hilbert space (see [25]). However, the purpose of the remaining paper is to illustrate for a particular magnetic model that the ratios of the scalar weights  $w_i/w_0$  make it possible to truncate the sum to values  $\chi$  much smaller than the dimension of the Fock space, while low-lying single-particle quantum skyrmion states are still well approximated by  $\hat{b}_{i,\chi}^\dagger |0\rangle$ .

*Quantum Skyrmions in Chiral Magnets.*— We investigate a minimal model of a two-dimensional chiral magnet

$$\hat{H} = \sum_{\langle ij \rangle} \left( \sum_{\alpha=x,y,z} J_\alpha \hat{S}_{i,\alpha} \hat{S}_{j,\alpha} + \mathbf{D}_{ij} \cdot (\hat{S}_i \times \hat{S}_j) \right) + \sum_i \mathbf{B} \cdot \hat{S}_i \quad (6)$$

where  $\langle ij \rangle$  denotes a sum over pairs of neighboring sites (each pair is only summed over once). Unless otherwise mentioned, the operators  $\hat{S}_i$  are spin  $s = 1/2$  operators and we assume an interfacial Dzyaloshinskii–Moriya interaction with  $\mathbf{D}_{ij} = D\hat{e}_z \times \mathbf{r}_{ij}/a$  where  $a$  is the lattice constant and  $\mathbf{r}_{ij}$  the distance vector between two neighboring sites.

It has been shown that a system described by Eq. (6) hosts a variety of quantum skyrmion ground states [17, 19–21, 26, 27]. For small systems, finite-size effects are not negligible and the properties of the low-energy states can change dramatically with the choice of boundary conditions: open boundary conditions lead to helical magnetic spirals, field-polarized states, semiclassical skyrmions, liquids and lattices; periodic boundary conditions can give rise to a symmetric and translational invariant ground state [17]; while a quantum flake embedded in a classical spin field suppresses helical states and removes the chiral surface twist on the system boundary [26]. To avoid such boundary effects, we focus on a quantum flake embedded in a fully polarized classical spin field. The quantum spins are located on a finite subset  $\mathcal{Q}$  of the full lattice  $\mathcal{S}$ , i.e.,  $\mathcal{Q} = \{\mathbf{R}_i, i = 0, \dots, N-1\} \subset \mathcal{S}$ , and are described by Eq. (6). Moreover, we add the following term to account for the cou-

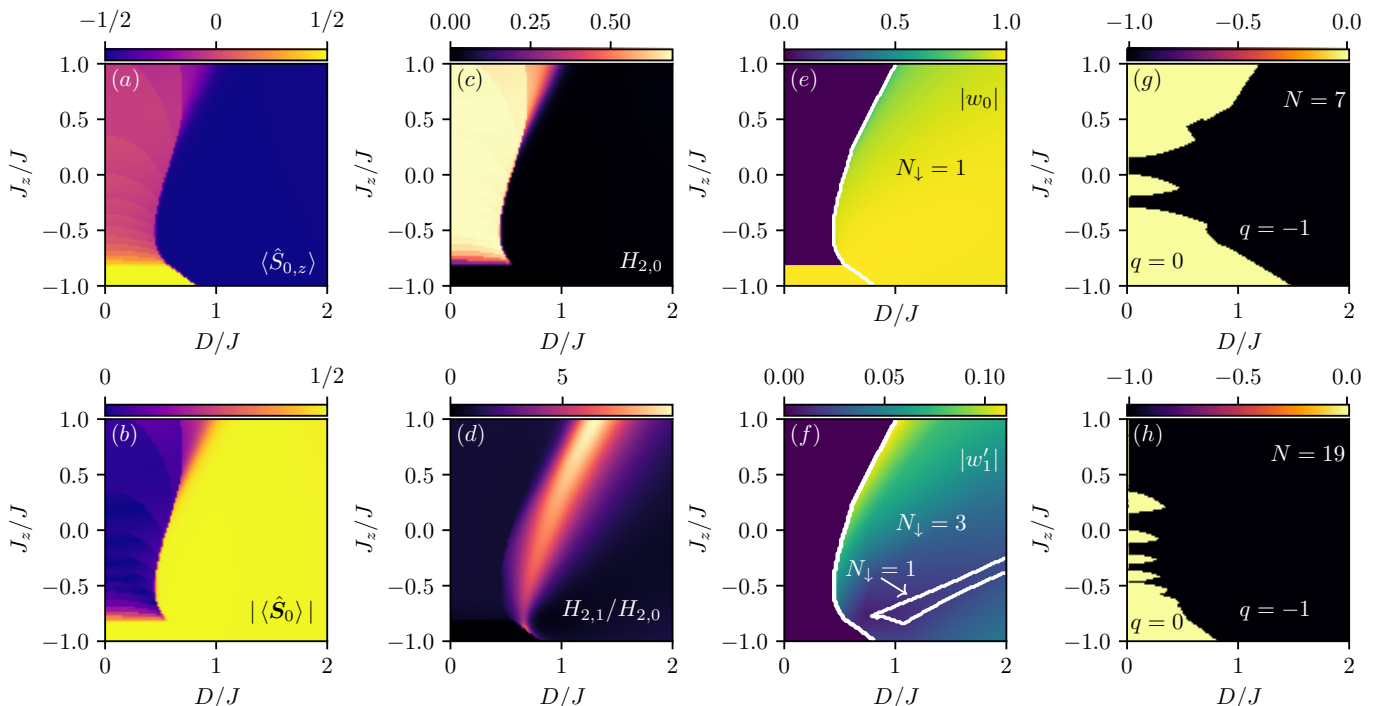


FIG. 2. Quantum magnetic skyrmions and other ground states supported by a finite-sized “quantum flake.” The quantum flake – a hexagonal region of the lattice of  $N$  spins with  $s = 1/2$  – is part of a chiral magnet embedded in a  $m_z = +1/2$  polarized classical environment. The Hamiltonian (7) models the coupling to the classical environment and Eq. (6) governs the chiral magnet, in which we use a vanishing Zeeman field  $B = 0$  and  $J_x = J_y = -J$  ( $J > 0$ ) for the exchange couplings. Varying the DMI amplitude  $D$  and the exchange coupling  $J_z$ , we use exact diagonalization to compute ground state quantities for  $N = 19$  sites: (a) expectation value of the central spin  $\langle \hat{S}_{0,z} \rangle$ ; (b) norm of the central spin  $|\langle \hat{S}_0 \rangle|$ ; (c) center second Rényi entropy  $H_{2,0}$ ; (d) ratio between off-center and center second Rényi entropies  $H_{2,1}/H_{2,0}$ ; probability amplitude magnitudes of (e) classical magnetic order  $|w_0|$  and (f) the six leading quantum corrections with equal amplitudes  $|w'_1| = w_1 = w_2 = \dots = w_6$ , defined in Eq. (9), from the ground state expanded in the rotated Fock state basis; and (g) topological charge of the ground state magnetization  $q$  (defined in [25]). In panel (h), we depict  $q$  for an  $N = 7$  quantum flake. Possible ground states: quantum skyrmion (blue region in (a) where  $\langle \hat{S}_{0,z} \rangle \approx -1/2$ ), field-polarized state (yellow region in (a) where  $\langle \hat{S}_{0,z} \rangle = +1/2$ ), and vortex state [pink region in (a) where  $\langle \hat{S}_{0,z} \rangle \approx 0$  with large quantum fluctuations indicated in (c)]. Contour lines and  $N_\downarrow = \sum_j n_{k,j}$  in (e) and (f) indicate, respectively, the region and the corresponding number of down spins. Probability amplitudes  $w_0$  and  $w_1$  are also the weights needed for the construction of the quantum skyrmion operator.

pling to the environment:

$$\hat{H}_{QC} = \sum_{\langle ij \rangle} \left( \sum_{\alpha=x,y,z} J_\alpha \hat{S}_{i,\alpha} m_{j,\alpha} + \mathbf{D}_{ij} \cdot (\hat{\mathbf{S}}_i \times \mathbf{m}_j) \right) \quad (7)$$

where the sites  $j$  are in the complement  $\mathcal{C} = \mathcal{S} \setminus \mathcal{Q}$  and  $\mathbf{m}_j = (m_{j,x}, m_{j,y}, m_{j,z})$  is a classical spin with length  $s$ .

For computational convenience, we consider finite triangular lattices with hexagonal  $C_6$  symmetry. We call the  $N = 7$  flake a single-shell and the  $N = 19$  flake a two-shell system, which allows us to investigate by exact diagonalization small  $C_6$  symmetric quantum skyrmions which have a maximal radius  $r_c \approx 3a$ . Some quantum properties of these states have already been investigated numerically in larger systems with open boundary conditions [21, 24], but quantifying the amount of quantum fluctuations, and how these fluctuations are affected by microscopic parameters, remains largely unexplored.

In the next section, we examine the skyrmion ground states  $|\psi\rangle$  obtained by exact diagonalization and perform a Fock state tomography which allows us to argue that the creation operator (3) indeed satisfies  $|\psi\rangle \approx \hat{b}_{0,\chi}^\dagger |0\rangle$ , where the quality of the approximation is controlled by  $\chi$ .

*Tomography of Quantum Skyrmions.* – Using exact diagonalization, we obtain the ground state diagram of Eq. (6) subject to the boundary conditions imposed by adding Eq. (7) and present our findings in Fig. 2. The state diagram we obtain here is qualitatively similar to that presented in a previous work [26], but it deserves further discussion. Our exact diagonalization simulations are performed with 19 sites on a triangular lattice whereas the previous work used 9 sites on a square lattice. Qualitatively, local spin expectation values allow a clear distinction between three regions: (i) a region hosting a field-polarized classical ground state indicated by a quantized spin expectation value norm  $s = |\langle \hat{S}_0 \rangle|$  in the

yellow regime of Fig. 2 (a), (ii) a vortex region with large quantum fluctuations signaled by vanishing center spin expectation value  $|\langle \hat{S}_0 \rangle| \approx 0$  and center Rényi entropy  $H_{2,0} \approx \ln 2$  displayed in Fig. 2 (b) and (c), and (iii) a quantum skyrmion regime which is indicated by the contour lines in panels (e) and (f). The quantum skyrmion region is also clearly indicated by an opposite magnetization order compared to the field-polarized environment, which is marked by the dark blue region in Fig. 2 (a), and a finite spin expectation value norm presented in panel (b). The field-polarized and quantum skyrmion states can further be distinguished by investigating the ratio between off-center and center Rényi entropy, defined by

$$H_\alpha(\rho_A) = \frac{1}{1-\alpha} \text{tr} \ln(\rho_A^\alpha), \quad \rho_A = \text{tr}_{A^C} |\psi\rangle\langle\psi|, \quad (8)$$

where  $\rho_A$  is the reduced density matrix of a bipartition  $A \subseteq \mathcal{Q}$  and the trace is performed over the local basis of the complement  $A^C$ . In Fig. 2, panels (c) and (d), we show the second Rényi entropies for a single-spin bipartition  $A_i = \{\mathbf{R}_i\}$ , i.e.,  $H_{2,i} = H_2(\rho_{A_i})$ . In (c), the single spin is at the center of the flake, which we denote by  $A_0 = \{\mathbf{R}_0\}$  and  $H_{2,0}$ , whereas (d) presents the ratio between the off-center Rényi entropy  $H_{2,1}/H_{2,0}$ , where  $A_1 = \{\mathbf{R}_1\}$  denotes the bipartition choice of the off-center spin,  $|\mathbf{R}_1 - \mathbf{R}_0| = a$ . Due to the six-fold rotation symmetry of the flake, it is irrelevant which spin of the first outer rim of the center is chosen. The ratio  $H_{2,1}/H_{2,0}$  is displayed in Fig. 2 (d). It indicates that the off-center spins of the skyrmion texture can be more entangled with the rest of the quantum system than the center spin. This is compatible with the entanglement properties found for skyrmions of larger systems [21, 24, 28]. We want to emphasize here that the field-polarized states are product states, indicated by vanishing Rényi entropy for every spin, whereas quantum skyrmion states display small but non-vanishing Rényi entropy. Although the state boundaries between vortex and magnetically ordered states (yellow and blue regions of Fig. 2 (b)) are slightly shifted upon varying the system geometry, we find that the qualitative features of the magnetically ordered states in the yellow region of panel (b) remain the same, and therefore finite size effects are marginal. In contrast, the vortex states of the blue region in Fig. 2 (b) are characterized by near-maximal center site Rényi entropy (displayed in Fig. 2 (c)) and almost vanishing spin expectation norm. Previous work identified some states in the  $q = -1$  lobes of panels Fig. 2 (g) and (h) of the vortex region as quantum skyrmions due to the possibility of defining a quantized topological charge [26]. However, the form of the magnetic profile and the resulting topological charge of the regions with small non-vanishing spin expectations depend strongly on the geometry of the quantum system. We thus focus on a detailed investigation of the unambiguously ordered quantum skyrmion states, for which the quantum skyrmion operator is most relevant. Due to the  $C_6$  symmetry of the lattice, we can expand the wave function in a ro-

tated Fock basis [25], and sort the weights by absolute magnitude. These weights can be extracted from the state obtained by exact diagonalization, and are shown in Fig. 2 (e, f). Depending on the parameters of the system, we find that the ground state wave functions assume two qualitatively different forms, which we denote as  $|\Psi_I\rangle$  and  $|\Psi_{II}\rangle$ , i.e.,

$$\begin{aligned} |\Psi_I\rangle &= \hat{R}_0 \left( w_0 \left| \begin{array}{c} \text{flake with 6 purple spins} \end{array} \right\rangle + w'_1 \sum_{n=0}^5 \hat{C}_6^n \left| \begin{array}{c} \text{flake with 6 purple spins, 1 yellow spin} \end{array} \right\rangle \right) + \dots \\ |\Psi_{II}\rangle &= \hat{R}_0 \left( w_0 \left| \begin{array}{c} \text{flake with 6 purple spins, 1 yellow spin} \end{array} \right\rangle + w'_1 \sum_{n=0}^5 \hat{C}_6^n \left| \begin{array}{c} \text{flake with 6 purple spins} \end{array} \right\rangle \right) + \dots \end{aligned} \quad (9)$$

where we retained the classical magnetic configuration  $w_{k=0}$  as well as the six leading quantum corrections with equal weights  $|w'_1| = |w_j|$  for  $j = 1, \dots, 6$ . Here,  $\hat{C}_6$  denotes the operator associated with a  $\pi/3$  rotation of the Fock state [25]. The graphical notation indicates the position of the spin flips associated with  $\mathbf{n}_k$ : purple denotes  $\uparrow$  spins ( $n_{k,j} = 0$ ), yellow denotes  $\downarrow$  occupation ( $n_{k,j} = 1$ ), and the rotation onto the classical magnetic order is incorporated in the operator  $\hat{R}_0$ . Notably, the rotated Fock state expansion reveals that the dominant corrections to the classical magnetic order involve only an odd number of down spins, as visible in the  $N_\downarrow = \{1, 3\}$  regions of panel (f). More interestingly, the leading quantum corrections with prefactor  $|w'_1|$  can take two qualitatively different forms: The leading quantum corrections in  $|\Psi_I\rangle$  are generated from  $N_\downarrow = 3$  states, whereas subleading quantum corrections stem from  $N_\downarrow = 1$  states. Instead, in  $|\Psi_{II}\rangle$ , the leading corrections stem from  $N_\downarrow = 1$  states. Therefore, we conclude that the semiclassical skyrmion phase hosts at least two different types of quantum skyrmions, which have the same classical order but differ in their quantum corrections. Compared to the classical ordered state, the fluctuations in the subleading term of  $|\Psi_I\rangle$  involve flipped spins surrounding the skyrmion center, whereas in  $|\Psi_{II}\rangle$  they include the spin at the skyrmion center and one of its neighboring spins. In panels (e) and (f), we plot  $|w_0|$  and  $|w'_1|$ , respectively, together with the associated sum of down-spin occupations  $N_\downarrow = \sum_j n_{k,j}$ . Contour lines mark the domain of the occupation sectors, and we see that  $w_0$  with  $N_\downarrow = 1$  extends over the full skyrmion bubble in the state diagram. Clearly  $N_\downarrow = 1$  terms are not the dominant corrections in the major part of the ground state diagram (see Fig. 2 (f)). Given that the results reveal only comparatively small quantum fluctuations around an ordered state, it would be interesting to compare the results presented here with the outcomes of spin wave theory calculations, in particular in the form of magnon squeezed states [29].

Finally, we want to highlight that our Fock state expansion could be used as a variational ansatz for the wave function of semiclassical quantum skyrmions, which potentially leads to performant numerical optimization al-

gorithms. The classical magnetic order can be captured by 2 rotation angles per site, resulting in 38 parameters for the 19-site quantum flake that minimize the classical energy, i.e.,

$$E_c = \min_{\boldsymbol{\theta}, \boldsymbol{\phi}} \langle \Psi_c(\boldsymbol{\theta}, \boldsymbol{\phi}) | \hat{H} | \Psi_c(\boldsymbol{\theta}, \boldsymbol{\phi}) \rangle. \quad (10)$$

In addition,  $\chi + 1$  complex weights represent the quantum fluctuations. In the semiclassical skyrmion regime, we see in Fig. 2 panels (e) and (f) that  $\chi = 6$  approximates the ground state with almost constant fidelity because the leading quantum fluctuations, contributing with amplitudes  $|w'_1|$ , compensate for the decrease of the classical contribution  $w_0$ . We noticed that  $w_1$  to  $w_6$  are equal in amplitude, and can be captured by the single parameter  $w'_1$  up to phases originating from  $\hat{C}_6$  rotations, which reduces the number of different weights from 7 to 2 without sacrificing fidelity. For comparison, we can estimate the number of variational parameters of an unconstrained matrix product state (MPS) simulation. We find that comparable wave function fidelities are reached with bond dimension  $M = 3$ , which corresponds to MPSs with 314 complex variational parameters [24]. The rotated Fock states are thus potentially useful to implement a more efficient constrained computational basis for variational optimization algorithms.

*Summary and Conclusion.*— In this paper, we introduced a variational ansatz to represent quantum skyrmions as bosonic operators. The form of this operator is determined by the desire to represent faithfully two fundamentally different aspects of a quantum skyrmions:

the classical magnetic order and a “quantum cloud” of local spin-flip excitations around the classical magnetic order. Using a minimal model for a chiral magnet in two dimensions, we found two distinct regions in the single-skyrmion phase: one where the leading quantum corrections around the classical magnetic order contain a flip of the center spin and one where they only contain spin flips around the skyrmion center. We argued that the Fock basis of spin flips around the classical order can be particularly useful for numerical algorithms based on the variational principle, because limiting the allowed number of spin flips truncates the dimension of the numerical Fock space and thus reduces the amount of free parameters in the simulations. We expect that such approaches can be fruitful when applied to or combined with tensor network simulations. Our work therefore paves the way toward a coarse-grained bosonic description of many-skyrmion quantum phases such as quantum skyrmion liquids which, unlike other approaches, incorporates individual skyrmions’ microscopic quantum fluctuations.

*Acknowledgements.*— We thank Alexander Mook, Thore Posske, Matteo Rizzi, Karin Everschor-Sitte and Niklas Tausendpfund for stimulating discussions. T.L.S. and A.H. acknowledge financial support from the National Research Fund Luxembourg under Grants No. CORE C20/MS/14764976/TopRel and No. INTER/17549827/AndMTI. S.D. and W.B. acknowledge funding by the Excellence Strategy of the University of Konstanz via a Blue Sky project and by the Deutsche Forschungsgemeinschaft (DFG, German Research Foundation) via the Collaborative Research Center SFB 1432 project no. 425217212 and SPP2244 project no. 417034116.

- 
- [1] A. Bogdanov and D. Yablonskii, Thermodynamically stable “vortices” in magnetically ordered crystals. The mixed state of magnets, *Zh. Eksp. Teor. Fiz* **95**, 182 (1989).
  - [2] A. Bogdanov and A. Hubert, Thermodynamically stable magnetic vortex states in magnetic crystals, *Journal of Magnetism and Magnetic Materials* **138**, 255 (1994).
  - [3] U. K. Röbler, A. N. Bogdanov, and C. Pfleiderer, Spontaneous Skyrmion Ground States in Magnetic Metals, *Nature* **442**, 797 (2006).
  - [4] A. Neubauer, C. Pfleiderer, B. Binz, A. Rosch, R. Ritz, P. G. Niklowitz, and P. Böni, Topological Hall Effect in the A Phase of MnSi, *Phys. Rev. Lett.* **102**, 186602 (2009).
  - [5] K. Everschor-Sitte, J. Masell, R. M. Reeve, and M. Kläui, Perspective: Magnetic skyrmions — Overview of recent progress in an active research field, *Journal of Applied Physics* **124**, 240901 (2018).
  - [6] S. Heinze, K. von Bergmann, M. Menzel, J. Brede, A. Kubetzka, R. Wiesendanger, G. Bihlmayer, and S. Blügel, Spontaneous Atomic-Scale Magnetic Skyrmion Lattice in Two Dimensions, *Nature Physics* **7**, 713 (2011).
  - [7] N. Nagaosa and Y. Tokura, Topological properties and dynamics of magnetic skyrmions, *Nature Nanotechnology* **8**, 899–911 (2013).
  - [8] C. Psaroudaki and C. Panagopoulos, Skyrmion qubits: A new class of quantum logic elements based on nanoscale magnetization, *Phys. Rev. Lett.* **127**, 067201 (2021).
  - [9] J. Xia, X. Zhang, X. Liu, Y. Zhou, and M. Ezawa, Universal quantum computation based on nanoscale skyrmion helicity qubits in frustrated magnets, *Phys. Rev. Lett.* **130**, 106701 (2023).
  - [10] J. Nothhelfer, S. A. Díaz, S. Kessler, T. Meng, M. Rizzi, K. M. D. Hals, and K. Everschor-Sitte, Steering majorana braiding via skyrmion-vortex pairs: A scalable platform, *Phys. Rev. B* **105**, 224509 (2022).
  - [11] S. A. Díaz, J. Klinovaja, D. Loss, and S. Hoffman, Majorana bound states induced by antiferromagnetic skyrmion textures, *Phys. Rev. B* **104**, 214501 (2021).
  - [12] S. M. Vlasov, P. F. Bessarab, I. S. Lobanov, M. N. Potkina, V. M. Uzdin, and H. Jónsson, Magnetic skyrmion annihilation by quantum mechanical tunneling, *New Journal of Physics* **22**, 083013 (2020).
  - [13] S. A. Díaz and D. P. Arovas, Quantum nucleation of skyrmions in magnetic films by inhomogeneous fields, in *Memorial Volume for Shoucheng Zhang*, Chap. 2, pp. 19–

- 33.
- [14] C. Psaroudaki, S. Hoffman, J. Klinovaja, and D. Loss, Quantum dynamics of skyrmions in chiral magnets, *Phys. Rev. X* **7**, 041045 (2017).
- [15] H. Ochoa and Y. Tserkovnyak, Quantum skyrmionics, *International Journal of Modern Physics B* **33**, 1930005 (2019).
- [16] V. Lohani, C. Hickey, J. Masell, and A. Rosch, Quantum skyrmions in frustrated ferromagnets, *Phys. Rev. X* **9**, 041063 (2019).
- [17] O. M. Sotnikov, V. V. Mazurenko, J. Colbois, F. Mila, M. I. Katsnelson, and E. A. Stepanov, Probing the topology of the quantum analog of a classical skyrmion, *Phys. Rev. B* **103**, L060404 (2021).
- [18] O. M. Sotnikov, E. A. Stepanov, M. I. Katsnelson, F. Mila, and V. V. Mazurenko, Emergence of classical magnetic order from anderson towers: Quantum darwinism in action, *Phys. Rev. X* **13**, 041027 (2023).
- [19] V. Vijayan, L. Chotorlishvili, A. Ernst, S. S. P. Parkin, M. I. Katsnelson, and S. K. Mishra, Topological dynamical quantum phase transition in a quantum skyrmion phase, *Phys. Rev. B* **107**, L100419 (2023).
- [20] V. V. Mazurenko, I. A. Iakovlev, O. M. Sotnikov, and M. I. Katsnelson, Estimating patterns of classical and quantum skyrmion states, *Journal of the Physical Society of Japan* **92**, 10.7566/jpsj.92.081004 (2023).
- [21] A. Joshi, R. Peters, and T. Posske, Ground state properties of quantum skyrmions described by neural network quantum states, *Phys. Rev. B* **108**, 094410 (2023).
- [22] A. Joshi, R. Peters, and T. Posske, Quantum skyrmion dynamics studied by neural network quantum states (2024), [arXiv:2403.08184 \[cond-mat.dis-nn\]](https://arxiv.org/abs/2403.08184).
- [23] R. Peters, J. Neuhaus-Steinmetz, and T. Posske, Quantum skyrmion hall effect in  $f$ -electron systems, *Phys. Rev. Res.* **5**, 033180 (2023).
- [24] A. Haller, S. Groenendijk, A. Habibi, A. Michels, and T. L. Schmidt, Quantum skyrmion lattices in heisenberg ferromagnets, *Phys. Rev. Res.* **4**, 043113 (2022).
- [25] See the Supplemental Material at ... where we discuss details of the rotated Fock state basis, fidelity, topological charge, and adiabatic exchange of two semi-classical skyrmions.
- [26] P. Siegl, E. Y. Vedmedenko, M. Stier, M. Thorwart, and T. Posske, Controlled creation of quantum skyrmions, *Phys. Rev. Res.* **4**, 023111 (2022).
- [27] F. Salvati, M. I. Katsnelson, A. A. Bagrov, and T. Westerhout, Stability of a quantum skyrmion: Projective measurements and the quantum zeno effect, *Phys. Rev. B* **109**, 064409 (2024).
- [28] D. Bhowmick, A. Haller, D. S. Kathyat, T. L. Schmidt, and P. Sengupta, Quantum skyrmion liquid (2023).
- [29] A. Kamra, E. Thingstad, G. Rastelli, R. A. Duine, A. Brataas, W. Belzig, and A. Sudbø, Antiferromagnetic magnons as highly squeezed fock states underlying quantum correlations, *Phys. Rev. B* **100**, 174407 (2019).
- [30] A. Perelomov, *Generalized Coherent States and Their Applications*, Theoretical and Mathematical Physics (Springer Berlin Heidelberg, 2012).
- [31] B. Berg and M. Lüscher, Definition and statistical distributions of a topological number in the lattice  $o(3)$  sigma-model, *Nuclear Physics B* **190**, 412 (1981).
- [32] M. V. Berry, Quantal phase factors accompanying adiabatic changes, *Proceedings of the Royal Society of London. A. Mathematical and Physical Sciences* **392**, 45–57 (1984).
- [33] C. Nayak, S. H. Simon, A. Stern, M. Freedman, and S. Das Sarma, Non-abelian anyons and topological quantum computation, *Rev. Mod. Phys.* **80**, 1083 (2008).
- [34] R. A. Istomin and A. S. Moskvina, Overlap integral for quantum skyrmions, *Journal of Experimental and Theoretical Physics Letters* **71**, 338–341 (2000).

# Supplemental Materials for “Quantum Magnetic Skyrmion Operator”

## I. ROTATED FOCK STATES

In this section, we construct a suitable orthonormal basis to expand the quantum skyrmion states with a semi-classical spin profile. A classical skyrmion without quantum fluctuations can be written as a product of spin coherent states [30]

$$|\Psi_c\rangle = \hat{R}(\boldsymbol{\theta}, \phi) |\uparrow\rangle \quad (\text{S1})$$

where  $\hat{R}$  is a product of local spin rotations, denoted by the polar  $\boldsymbol{\theta}$  and azimuth angles  $\phi$ , and  $|\uparrow\rangle$  represents the fully polarized spin state, i.e.

$$|\uparrow\rangle = \bigotimes_i |\uparrow\rangle_i, \quad \hat{R}(\boldsymbol{\theta}, \phi) = \prod_i e^{-i\phi_i \hat{S}_{i,z}} e^{-i\theta_i \hat{S}_{i,y}}. \quad (\text{S2})$$

We find that the best classical approximation to the quantum skyrmion state is obtained by a rotation operator which redirects the normalized spins of the ordered product state along the direction of the spin expectation values of the quantum state. We denote this product state as  $|\Psi_c\rangle$ , which is equivalent to  $|\uparrow\rangle$  up to local spin rotations by definition. Note that in this convention,  $|\Psi_c\rangle$  corresponds to a mean-field approximation of the ground state where all quantum fluctuations are neglected. Depending on the amount of quantum entanglement in the ground states, we find overlaps  $|w_0| := |\langle\Psi_c|\Psi\rangle| > 80\%$  in the yellow regions of (e): (i) The polarized states found in the bottom left region are equivalent to product states  $|\uparrow\rangle$ , whereas skyrmion ground states with finite entanglement (shades of green) display  $|w_0| < 1$ . In the complement region, large quantum fluctuations in the ground state result in magnetic textures without local order, which is indicated by panel (e) in the pillar-shaped region where the norm of the spin expectation value is vanishing  $|\langle\hat{S}_i\rangle| \approx 0$ . With exact diagonalization, it is hard to verify whether the eigenstates in this region assume a finite spin norm in larger systems, but a limited finite-size extrapolation (different sizes and system shapes) we can perform suggests a vanishing spin norm in the thermodynamic limit. Therefore, we expect the overlap to a product state to vanish exactly whenever  $|\langle\hat{S}_i\rangle| \rightarrow 0$  in the thermodynamic limit, marking a clear indicator when the employed Ansatz of Eq. (3) fails.

Quantum effects in the magnetically ordered ground states can be taken into account by expanding the quantum wave function in the basis of locally spin-flipped states, i.e.

$$|\mathbf{n}\rangle = \prod_i (\hat{S}_i^-)^{n_i} |\uparrow\rangle \quad (\text{S3})$$

where  $\mathbf{n} \in \{0, 1\}^{\otimes N}$  is a vector of occupation numbers associated with the total number and position of down spins. The Fock basis  $\{|\mathbf{n}_i\rangle\}$  spans a complete basis for the Hilbert space associated with  $\hat{H}$ . Note that the central spin of a skyrmion is anti-aligned with the order of the classical environment, and therefore any overlap  $\langle\mathbf{n}_i|\Psi\rangle$  vanishes.

This issue is overcome by using a *rotated* Fock basis where the local spin flips are aligned with the canonical axis of the magnetic order  $\{\hat{R}|\mathbf{n}_i\rangle\}$ . In this basis, the Fock state with the highest overlap to the true ground state  $w_0 := \langle\Psi_c|\Psi\rangle$  is given by  $|\Psi_c\rangle = \hat{R}|0\rangle = \hat{R}|\uparrow\rangle$ . Here and in the following, we assume that the lattice is commensurate with the skyrmion center, i.e. that the discretized skyrmion profile is spin-flipped at a lattice node with respect to the polarized environment. In this case, we can conveniently associate a lattice node with the center-of-mass of the skyrmion, which is highlighted more explicitly by replacing the central rotation in  $\hat{R}$  by a spin ladder operator, i.e.  $\hat{R} \rightarrow \hat{R}_0 \hat{S}_0^-$ . We now expand the wave function in the rotated Fock basis, which can be written in general as

$$|\Psi\rangle = \hat{R}_0 \sum_{i=0}^{\chi'} w_i |\mathbf{n}_i\rangle. \quad (\text{S4})$$

$\chi'$  denotes the number of states, and in principle is growing exponentially in the number of sites, i.e.  $\chi' = 2^N$ . We can, however, attempt to approximate any state by ordering the weights  $|w_i|$  by absolute magnitude, and truncate the sum to a smaller  $\chi < \chi'$ . Using exact diagonalization, we find a large regime in the state diagram which hosts quantum skyrmions (see Fig. 2), which is divided into two qualitatively different quantum skyrmion flavors, described by  $|\Psi_I\rangle$  and  $|\Psi_{II}\rangle$  of the main text. We here provide further subleading contributions of  $|\Psi_I\rangle$ , which corresponds to the state in the majority of the quantum skyrmion region:

$$|\Psi_I\rangle = \hat{R}_0 \left( w_0 \left| \begin{array}{c} \bullet \\ \bullet \\ \bullet \\ \bullet \\ \bullet \\ \bullet \\ \bullet \\ \bullet \\ \bullet \\ \bullet \end{array} \right\rangle + \sum_{n=0}^5 \hat{C}_6^n \left\{ w'_1 \left| \begin{array}{c} \bullet \\ \bullet \\ \bullet \\ \bullet \\ \bullet \\ \bullet \\ \bullet \\ \bullet \\ \bullet \\ \bullet \end{array} \right\rangle + w'_2 \left| \begin{array}{c} \bullet \\ \bullet \\ \bullet \\ \bullet \\ \bullet \\ \bullet \\ \bullet \\ \bullet \\ \bullet \\ \bullet \end{array} \right\rangle + \left[ w'_3 \left| \begin{array}{c} \bullet \\ \bullet \\ \bullet \\ \bullet \\ \bullet \\ \bullet \\ \bullet \\ \bullet \\ \bullet \\ \bullet \end{array} \right\rangle + w'_3{}^* \left| \begin{array}{c} \bullet \\ \bullet \\ \bullet \\ \bullet \\ \bullet \\ \bullet \\ \bullet \\ \bullet \\ \bullet \\ \bullet \end{array} \right\rangle \right] \right\} \right) + \dots \quad (\text{S5})$$

Similarly to the main text, we identify equal amplitudes with  $w'_i$ , i.e.  $|w'_1| = |w_1| = \dots = |w_6|$ ,  $|w'_2| = |w_7| = \dots = |w_{12}|$  and similarly for  $w'_3$ . The rotation operator  $\hat{C}_6$  acts on the spin-flipped Fock states in the following way

$$\hat{C}_6^5 \left| \begin{array}{c} \text{hexagon} \\ \text{with 6 purple dots} \end{array} \right\rangle = e^{i\pi/3} \hat{C}_6^4 \left| \begin{array}{c} \text{hexagon} \\ \text{with 6 purple dots} \end{array} \right\rangle = e^{2i\pi/3} \hat{C}_6^3 \left| \begin{array}{c} \text{hexagon} \\ \text{with 6 purple dots} \end{array} \right\rangle = \dots = e^{5i\pi/3} \left| \begin{array}{c} \text{hexagon} \\ \text{with 6 purple dots} \end{array} \right\rangle \quad (\text{S6})$$

$$\hat{C}_6^5 \left| \begin{array}{c} \text{hexagon} \\ \text{with 6 purple dots and 1 yellow dot} \end{array} \right\rangle = \hat{C}_6^4 \left| \begin{array}{c} \text{hexagon} \\ \text{with 6 purple dots and 1 yellow dot} \end{array} \right\rangle = \hat{C}_6^3 \left| \begin{array}{c} \text{hexagon} \\ \text{with 6 purple dots and 1 yellow dot} \end{array} \right\rangle = \hat{C}_6^2 \left| \begin{array}{c} \text{hexagon} \\ \text{with 6 purple dots and 1 yellow dot} \end{array} \right\rangle = \hat{C}_6^1 \left| \begin{array}{c} \text{hexagon} \\ \text{with 6 purple dots and 1 yellow dot} \end{array} \right\rangle = \left| \begin{array}{c} \text{hexagon} \\ \text{with 6 purple dots and 1 yellow dot} \end{array} \right\rangle \quad (\text{S7})$$

$$\hat{C}_6^5 \left| \begin{array}{c} \text{hexagon} \\ \text{with 6 purple dots and 2 yellow dots} \end{array} \right\rangle = \hat{C}_6^4 \left| \begin{array}{c} \text{hexagon} \\ \text{with 6 purple dots and 2 yellow dots} \end{array} \right\rangle = \hat{C}_6^3 \left| \begin{array}{c} \text{hexagon} \\ \text{with 6 purple dots and 2 yellow dots} \end{array} \right\rangle = \hat{C}_6^2 \left| \begin{array}{c} \text{hexagon} \\ \text{with 6 purple dots and 2 yellow dots} \end{array} \right\rangle = \hat{C}_6^1 \left| \begin{array}{c} \text{hexagon} \\ \text{with 6 purple dots and 2 yellow dots} \end{array} \right\rangle = \left| \begin{array}{c} \text{hexagon} \\ \text{with 6 purple dots and 2 yellow dots} \end{array} \right\rangle \quad (\text{S8})$$

$$\hat{C}_6^5 \left| \begin{array}{c} \text{hexagon} \\ \text{with 6 purple dots and 3 yellow dots} \end{array} \right\rangle = \hat{C}_6^4 \left| \begin{array}{c} \text{hexagon} \\ \text{with 6 purple dots and 3 yellow dots} \end{array} \right\rangle = \hat{C}_6^3 \left| \begin{array}{c} \text{hexagon} \\ \text{with 6 purple dots and 3 yellow dots} \end{array} \right\rangle = \hat{C}_6^2 \left| \begin{array}{c} \text{hexagon} \\ \text{with 6 purple dots and 3 yellow dots} \end{array} \right\rangle = \hat{C}_6^1 \left| \begin{array}{c} \text{hexagon} \\ \text{with 6 purple dots and 3 yellow dots} \end{array} \right\rangle = \left| \begin{array}{c} \text{hexagon} \\ \text{with 6 purple dots and 3 yellow dots} \end{array} \right\rangle \quad (\text{S9})$$

## II. OBSERVABLES

To evaluate the reliability of the above approximation, we make use of several observables, such as the fidelity between two arbitrary states  $|\Psi\rangle$  and  $|\Phi\rangle$

$$F(\Psi, \Phi) = |\langle \Psi | \Phi \rangle| \quad (\text{S10})$$

which will be the most reliable quantity to estimate the quality of an approximation. In particular, the fidelity of the approximation when we truncate the sum in Eq. (S4) is equal to the squared sum of weights  $F(\Psi|_\chi, \Psi) = \sum_{i=0}^X |w_i|^2 \leq 1$ . In Fig. 2 panels (e) and (f), we see that a reasonable state fidelity is reached by keeping only the first leading contributions,  $w_0$  and  $w_1$ . To investigate the magnetic texture, we compute the local spin expectation values

$$\mathbf{S}_i = \langle \hat{\mathbf{S}}_i \rangle \quad (\text{S11})$$

which, if  $|\mathbf{S}_i| \approx s$ , indicates magnetically ordered states. In such cases, the magnetic order is characterized by an integer number derived from the normalized spin expectation values  $\mathbf{O}_i = \mathbf{S}_i/|\mathbf{S}_i|$ , i.e.

$$q = \frac{1}{2\pi} \sum_{\langle ijk \rangle} \arg \left( \frac{X_{ijk} + iY_{ijk}}{\sqrt{X_{ijk}^2 + Y_{ijk}^2}} \right), \quad (\text{S12})$$

$$X_{ijk} = 1 + \mathbf{O}_i \cdot \mathbf{O}_j + \mathbf{O}_j \cdot \mathbf{O}_k + \mathbf{O}_k \cdot \mathbf{O}_i, \quad (\text{S13})$$

$$Y_{ijk} = \mathbf{O}_i \cdot (\mathbf{O}_j \times \mathbf{O}_k), \quad (\text{S14})$$

where  $\langle ijk \rangle$  denotes a sum over elementary triangles of the lattice [31]. The index  $q \in \mathbb{Z}$  is commonly denoted as ‘‘topological charge’’ and non-zero for magnetic skyrmion textures. Trivially ordered phases such as, e.g. field-polarized or in other collinear states, assume a vanishing charge  $q = 0$ .

## III. ADIABATIC EXCHANGE OF TWO SEMI-CLASSICAL SKYRMIONS WITH MPS

One characteristic quantity related to the elementary form of a quantum mechanical many-body wave function is the statistical phase after particle exchange. In particular, a wave function of two bosons (fermions)  $\Psi(\mathbf{x}_1, \mathbf{x}_2)$  with  $\mathbf{x}_1 \neq \mathbf{x}_2$  the different positions of the two particles acquires a statistical phase  $+1$  ( $-1$ ) after particle exchange  $\Psi(\mathbf{x}_1, \mathbf{x}_2) \rightarrow \Psi(\mathbf{x}_2, \mathbf{x}_1) = \pm \Psi(\mathbf{x}_1, \mathbf{x}_2)$ . A geometric way to obtain the exchange phase is through the Berry phase [32, 33]. To compute the Berry phase, we need to define a closed path in parameter space of the Hamiltonian  $\hat{H}(\lambda)$  such that  $\hat{H}(\lambda_i) = \hat{H}(\lambda_f)$ , such that  $\Psi(\mathbf{x}_1, \mathbf{x}_2)$  and  $\Psi(\mathbf{x}_2, \mathbf{x}_1)$  are the unique ground state wave functions of two skyrmions located around the center-of-mass positions  $\mathbf{x}_1$  and  $\mathbf{x}_2$  at  $\lambda_i$  and  $\lambda_f$ . If  $\lambda(t)$  is changed adiabatically in time, we can assume that the ground state  $\Psi$  follows the parameter deformation instantaneously, such that  $|\Psi(t)\rangle = |\Psi(\lambda)\rangle$ . Additionally, the energy gap between the ground and the first excited state must stay finite during the deformation. We realize the parameter deformation by an additional pinning potential

$$\hat{V}(\lambda) = V_0 \sum_{j=1}^N \sum_{i=1}^2 \exp \left( -\frac{|\mathbf{R}_j - \mathbf{x}_i(\lambda)|^2}{2\sigma^2} \right) \hat{S}_{z,j} \quad (\text{S15})$$



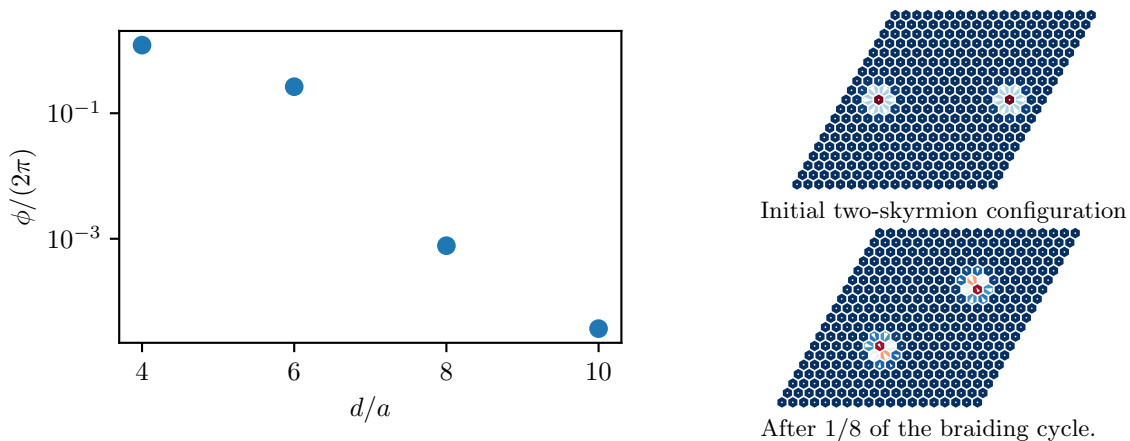


FIG. S1. Exchange angle versus distance for a semi-classical profile with two skyrmions using a strong pinning field  $V_0 = 4J$ ,  $\sigma = a$ .

on top of the Hamiltonian in Eq. (6). If the exchange couplings are tuned such that the ground state is polarized to the external field, adding a strong field  $V_0 \gg J$  pins exactly two semi-classical skyrmion profiles around the center-of-mass locations  $\mathbf{x}_1(\lambda)$  and  $\mathbf{x}_2(\lambda)$ . We then smoothly deform the pinning potential such that  $\mathbf{d}(\lambda) := \mathbf{x}_2(\lambda) - \mathbf{x}_1(\lambda)$  rotates by  $\pi$  in the interval  $\lambda \in [0, 1]$ , i.e.

$$\mathbf{d}(\lambda) = d \begin{pmatrix} \cos(\pi\lambda) \\ \sin(\pi\lambda) \end{pmatrix}. \quad (\text{S16})$$

For the smallest skyrmion profiles  $r_c \approx 3a$ , a well-separated two-skyrmion magnetization profile already requires system sizes which cannot be investigated by exact diagonalization. Instead, we proceed by using MPS simulations for larger quantum systems, which are known to faithfully capture the properties of semi-classical skyrmion lattice ground states [24]. The Berry phase is then extracted by (i) using variational MPS to evaluate the ground states of a discrete sequence in the adiabatic deformation, i.e.  $\{|\Psi_n\rangle := |\Psi(n\Delta\lambda)\rangle, n = 0, \dots, N_\lambda - 1\}$  with  $\Delta\lambda = 1/N_\lambda$ , and (ii) evaluating the Berry phase through a Wilson loop, i.e.

$$\phi = \arg \prod_n \frac{\langle \Psi_n | \Psi_{n+1} \rangle}{|\langle \Psi_n | \Psi_{n+1} \rangle|}. \quad (\text{S17})$$

It is easy to recognize that the Berry phase  $\phi$  obtained by the Wilson loop is invariant under gauge transforms  $|\Psi_n\rangle \rightarrow e^{i\varphi} |\Psi_n\rangle$  by definition, such that we do not need to fix a gauge for the numeric simulations. We present the outcomes of this numerical experiment in Fig. S1. From the quantum skyrmion operator, we expect that the exchange angle of quantum skyrmions is  $\text{mod}_{2\pi} 0$  for  $r > r_c$ , which seems to be compatible with the numerical results up to the reachable precision. It is therefore reasonable to argue that the two entities behave as bosonic quasiparticles if they are separated over large distances. On short distances comparable with the diameter of individual skyrmions, the exchange phase increases, which is also expected because the rotation operators onto the classical magnetic order overlap [34].